1-1-1991

A Mathematical Model of a Sealed Nickel-Cadmium Battery

Deyuan Fan
Texas A & M University - College Station

Ralph E. White
University of South Carolina - Columbia, white@cec.sc.edu

Publication Info

Journal of the Electrochemical Society, 1991, pages 17-25.

DOI: 10.1149/1.2085532
http://dx.doi.org/10.1149/1.2085532

Table A-II. Volume decrease during discharge for various electrolyte compositions (no membrane separator present)

x_k[a]	x_{Zn}[a]	ρ_z[a] kg · l^{-1}	x_{KOH}	ρ_l[b] kg · l^{-1}	V_2/V_1	V_3/V_1
0.0818	0.0055	1.1076	0.1201	1.1060	1.0015	0.0009
0.1500	0.0183	1.2258	0.2253	1.2065	0.9941	0.0031
0.2130	0.0361	1.3616	0.3275	1.3099	0.9812	0.0068
0.2190	0.0371	1.3637	0.3369	1.3198	0.9876	0.0070
0.2890	0.0634	1.5356	0.4576	1.4532	0.9799	0.0134
0.2480[c]	0.0495[c]	1.4720[c]	0.3875	1.3743	0.9592	0.0098
0.2900[c]	0.0679[c]	1.5890[c]	0.4622	1.4586	0.9528	0.0144
0.2960[c]	0.0781[c]	1.6530[c]	0.4784	1.4773	0.9331	0.0169

[a] Data from (13), 25°C.
[b] Compiled from (12), 20°C.
[c] Data from (14), 18°-20°C.

For example, in the presence of a weak cationic membrane separator, the transport numbers of K^+ and OH^- can be set equal (1). Assuming that along with one K^+ four water molecules are transported from the zinc electrode towards the nickel electrode compartment, the volume of the electrolyte in the zinc electrode compartment decreases significantly, as can be seen from Table A-I. If the membrane separator is omitted and only a quarter of the current is carried by K^+, a smaller decrease of the volume is observed (Table A-II).

In the actual battery system, the electrolyte in the zinc electrode compartment will not be completely depleted in zincate at the beginning of discharge. However, the electrolyte at the end of discharge will not be saturated but will be supersaturated with zincate. Furthermore, the properties of chemically and electrochemically formed zincate solutions are different (18, 19) and during discharge of the zinc electrode, apart from soluble zinc species, ZnO or related solid zinc compounds are formed. Therefore, the results in Table A-I and A-II must be taken in a qualitative sense: and it seems that in actual battery systems the volume of the electrolyte in the zinc electrode compartment decreases more than would be expected from the results in Table A-I and A-II.

REFERENCES

1. K. W. Choi, D. N. Bennion, and J. Newman, *This Journal*, **123,** 1616 (1976).
2. J. McBreen, *ibid.*, **119,** 1620 (1972).
3. K. W. Choi, D. N. Bennion, and J. Newman, *ibid.*, **123,** 1625 (1976).
4. K. W. Choi, Ph. D. Thesis, University of California, Los Angeles (1975).
5. R. G. Gunther and R. M. Bendert, *This Journal*, **134,** 782 (1987).
6. R. E. F. Einerhand, W. Visscher, J. J. M. de Goeij, and E. Barendrecht, *ibid.*, **138,** 1 (1991).
7. R. E. F. Einerhand, W. H. M. Visscher, E. Barendrecht, and J. J. M. de Goeij, p. 751 of Extended Abstracts of 38th ISE Meeting," Vol. 2, Maastricht, 1987.
8. E. H. Hietbrink and R. F. Hill, *This Journal*, **136,** 310 (1989).
9. J. McBreen and E. J. Cairns, in "Advances in Electrochemistry and Electrochemical Engineering," Vol. 11, H. Gerischer and C. W. Tobias, Editors, p. 273, John Wiley & Sons, Inc., New York (1978).
10. K. W. Choi, D. Hamby, D. N. Bennion, and J. Newman, *This Journal*, **123,** 628 (1976).
11. R. E. F. Einerhand, Ph.D. Thesis, Eindhoven University of Technology, Eindhoven (1989).
12. "Handbook of Chemistry and Physics," 62nd ed., CRC Press Inc., Boca Raton, FL (1981-1982).
13. T. P. Dirkse, *This Journal*, **106,** 154 (1959).
14. V. G. Sochevanov, *J. Gen. Chem. U.S.S.R.*, **22,** 1119 (1952).
15. D. C. Hamby, N. J. Hoover, J. Wirkkala, and D. Zahnle, *This Journal*, **126,** 2110 (1979).
16. M. J. Isaacson, F. R. McLarnon, and E. J. Cairns, Abstract 147, p. 214, The Electrochemical Society Extended Abstracts, Vol. 87-2, Honolulu, HI, Oct. 18-23, 1987.
17. R. E. F. Einerhand, Ph.D. Thesis, Chap. 5, pp. 83-98, Eindhoven University of Technology, Eindhoven (1989).
18. C. Cachet, B. Saidani, and R. Wiart, *Electrochim. Acta.*, **33,** 405 (1988).
19. V. E. Dmitrenko, M. S. Zukov, V. I. Baulov, and A. V. Kotov, *Sov. Electrochem.*, **19,** 1414 (1983).

A Mathematical Model of a Sealed Nickel-Cadmium Battery

Deyuan Fan* and Ralph E. White**

Department of Chemical Engineering, Texas A&M University, College Station, Texas 77843-3122

ABSTRACT

A mathematical model for the charge and discharge of a sealed nickel-cadmium (Ni-Cd) battery is presented. The model is used to study the effect of transport properties of the electrolyte and kinetic parameters of the electrode reactions on the cell performance during the charge and discharge period. The model can also be used to demonstrate the changes of cell performance during cycling. Some comparisons between model predictions and experimental results indicate that the model predictions appear to fit the experimental data well. Sensitivity analyses illustrate that the sealed nickel-cadmium battery operates under activation control. It is also shown theoretically that oxygen generated on the positive electrode during charge is reduced electrochemically on the negative electrode.

It is well known that the performance of a nickel-cadmium battery is based on the complex chemical and electrochemical phenomena (1-4) involved in the battery. These complex phenomena can be understood better through mathematical modeling of the battery. Similar work has been done for other battery systems such as the model for the nickel-zinc battery by Choi and Yao (5) and the model for the lead-acid battery by Gu *et al.* (6), both for flooded/vent conditions. In October 1989, Bouet and Richard (7) presented their discharge performance model for the nickel hydroxide electrode at the 176th Meeting of The Electrochemical Society. However, their model includes only the nickel positive electrode and does not include sealed cell conditions and the oxygen reaction. Recently, Nguyen *et al.* (8) proposed a mathematical model for the lead-acid battery under sealed conditions during discharge, but a model for predicting the cell performance under sealed conditions during charge has not been presented. To assist researchers and designers in the investigation and development of sealed nickel-cadmium batteries, a detailed mathematical model of a sealed, starved separator nickel-cadmium cell is presented here that can be used to predict the performance of a cell not only during discharge, but also during charge, rest, and cycling. A description of the model equations, qualitative comparisons between the model predictions and experimental re-

* Electrochemical Society Student Member.
** Electrochemical Society Active Member.

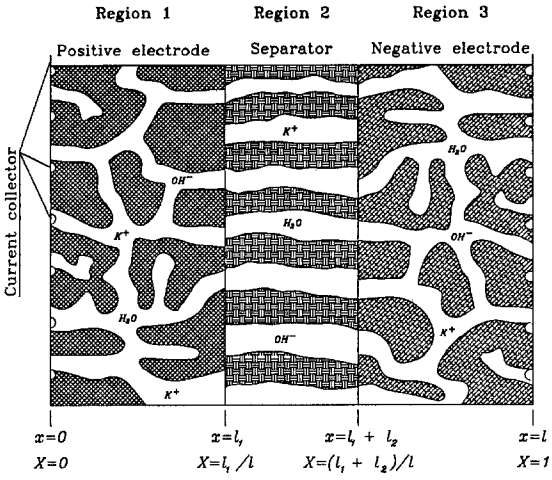

Fig. 1. A schematic of a hermetically sealed, starved separator, sinter plate nickel-cadmium cell (cross-sectional view).

sults, and sensitivity analyses of the model simulations to the model parameters are presented below.

Model Development

Although the detailed mechanisms of the electrode reactions in the nickel-cadmium cell are not thoroughly understood, it is generally agreed that the main electrode reactions in the cell can be written as (1-4, 9-13)

Positive Electrode

$$2NiOOH + 2H_2O + 2e^- \underset{\text{charge}}{\overset{\text{discharge}}{\rightleftharpoons}} 2Ni(OH)_2 + 2\,OH^- \quad [A]$$

$$\frac{1}{2}O_2 + H_2O + 2e^- \underset{\text{charge}}{\overset{\text{discharge}}{\rightleftharpoons}} 2\,OH^- \quad [B]$$

Negative Electrode

$$Cd + 2\,OH^- \underset{\text{charge}}{\overset{\text{discharge}}{\rightleftharpoons}} Cd(OH)_2 + 2e^- \quad [C]$$

$$2\,OH^- \underset{\text{charge}}{\overset{\text{discharge}}{\longrightarrow}} \frac{1}{2}O_2 + H_2O + 2e^- \quad [D]$$

A schematic of a sealed nickel-cadmium cell is shown in Fig. 1. The cell consists of the following regions and boundaries: (*i*) the current collector of the positive electrode ($x = 0$); (*ii*) the positive or nickel electrode (region 1, $0 < x < l_1$); (*iii*) the interface between the positive electrode and the separator ($x = l_1$); (*iv*) the separator matrix (region 2, $l_1 < x < l_1 + l_2$); (*v*) the interface between the separator and the negative electrode ($x = l_1 + l_2$); (*vi*) the negative or cadmium electrode (region 3, $l_1 + l_2 < x < l$); and (*vii*) the current collector the negative electrode ($x = l$).

There are six explicit unknowns (dependent variables) in the model; (*i*) base concentrations, c; (*ii*) solid material porosity, ϵ; (*iii*) potential in the solid phase, ϕ_1; (*iv*) potential in the liquid phase, ϕ_2; (*v*) superficial current density in the electrolyte, i_2; and (*vi*) oxygen concentration, c_{O_2}. The independent variables are the spatial coordinate x and time t.

The governing equations and the boundary conditions for these six variables for the nickel-cadmium cell are presented next. The concentrated solution theory has been used to derive these equations.

Center of the positive electrode.—

$$\frac{\partial c}{\partial x} = 0 \quad [1]$$

$$\frac{\partial \epsilon_1}{\partial t} = \frac{1}{\mathbf{F}}\left(\frac{M_{Ni(OH)_2}}{\rho_{Ni(OH)_2}} - \frac{M_{NiOOH}}{\rho_{NiOOH}}\right) j_{Ni} \quad [2]$$

$$i_2 = 0 \quad [3]$$

$$\frac{\partial \phi_2}{\partial x} = 0 \quad [4]$$

$$\phi_1 = 0 \quad [5]$$

$$\frac{\partial c_{O_2}}{\partial x} = 0 \quad [6]$$

where, on discharge and at rest

$$j_{Ni} = a_{max1} i_{o1,ref}\left(\frac{c}{c_{ref}}\right)^{\gamma 1}\left(\frac{\epsilon_1 - \epsilon_{o1}}{\epsilon_{max1} - \epsilon_{o1}}\right)^{\zeta 1} \left\{\exp\left[\frac{\alpha_{a1}\mathbf{F}}{RT}\eta_a\right] - \exp\left[\frac{-\alpha_{c1}\mathbf{F}}{RT}\eta_a\right]\right\} \quad [7a]$$

and on charge

$$j_{Ni} = a_{max1} i_{o1,ref}\left(\frac{c}{c_{ref}}\right)^{\gamma 1}\left(\frac{\epsilon_{max1} - \epsilon_1}{\epsilon_{max1} - \epsilon_{o1}}\right)^{\zeta 1} \left\{\exp\left[\frac{\alpha_{a1}\mathbf{F}}{RT}\eta_a\right] - \exp\left[\frac{-\alpha_{c1}\mathbf{F}}{RT}\eta_a\right]\right\} \quad [7b]$$

where

$$\eta_a = \phi_{1,Ni} - \phi_2 - U_{Ni/Cd} \quad [7c]$$

and

$$U_{Ni/Cd} = U_{NiOOH/Ni(OH)_2} - U_{Cd(OH)_2/Cd} = 1.299V \quad [7d]$$

Based on the cell construction in which the current collector is embedded in the center of a porous electrode (see Fig. 1), Eq. [1] and [6] are used to represent the condition that the flux of the electrolyte (KOH) and the flux of oxygen are both zero. Equation [2] is the governing equation for porosity changes of the nickel electrode, where the transfer current j_{Ni}, defined as $\partial i_2/\partial x$, is the local current per unit volume due to the electrode reaction. Equation [3] shows that at the center of the electrode all of the current leaves the liquid phase (electrolyte) and enters the solid phase (current collector). Consequently, the potential gradient in the liquid phase is equal to zero, Eq. [4]. The solid phase potential is arbitrarily set to zero at $x = 0$, Eq. [5]. Equations [7a] and [7b] are the kinetic expressions for the electrode reactions in the positive electrode. Equations [7c] and [7d] give the overpotential expression and the corresponding open-circuit (equilibrium) potential for the nickel-cadmium cell.

Region 1: positive electrode.—Ohm's law in the solution

$$\frac{i_2}{\kappa \epsilon_1^{exl}} = -\frac{\partial \phi_2}{\partial x} + \frac{RT}{\mathbf{F}}(1 - t_-^\circ)\frac{\partial \ln c}{\partial x} \quad [8]$$

Conservation of charge

$$i_2 - \sigma_{NiOOH}\,\epsilon_1^{exm1}\frac{\partial \phi_{1,NiOOH}}{\partial x} = i_{cell} \quad [9]$$

Transfer current

$$\frac{\partial i_2}{\partial x} = j_{Ni} + j_{O_2} \quad [10]$$

Porosity variation

$$\frac{\partial \epsilon_1}{\partial t} = \frac{1}{\mathbf{F}}\left(\frac{M_{Ni(OH)_2}}{\rho_{Ni(OH)_2}} - \frac{M_{NiOOH}}{\rho_{NiOOH}}\right) j_{Ni} \quad [11]$$

Electrolyte material balance

$$\epsilon_1 \frac{\partial c}{\partial t} + c\frac{\partial \epsilon_1}{\partial t} = \frac{\partial}{\partial x}\left(D\epsilon_1^{ex1}\frac{\partial c}{\partial x}\right) - \left(\frac{1-t_-^o}{\mathbf{F}}\right) j_{Ni} + \frac{t_-^o}{\mathbf{F}} j_{O_2} \quad [12]$$

Oxygen material balance

$$\epsilon_1 \frac{\partial c_{O_2}}{\partial t} + c_{O_2}\frac{\partial \epsilon_1}{\partial t} = \frac{\partial}{\partial x}\left(D_{O_2}\epsilon_1^{ex1}\frac{\partial c_{O_2}}{\partial x}\right) + \frac{1}{4\mathbf{F}} j_{O_2} \quad [13]$$

where the kinetic expression for oxygen reaction is

$$j_{O_2} = a_{max1} i'_{o1,ref}\left(\frac{\epsilon_1 - \epsilon_{o1}}{\epsilon_{max1} - \epsilon_{o1}}\right)^{\zeta 1}\left\{\exp\left[\frac{\alpha'_a \mathbf{F}}{RT}\eta'_a\right] - \left(\frac{c_{O_2}}{c_{O_2,ref}}\right)\exp\left[\frac{-\alpha'_c \mathbf{F}}{RT}\eta'_a\right]\right\} \quad [14a]$$

where

$$\eta'_a = \phi_{1,Ni} - \phi_2 - U_{O_2/Cd} \quad [14b]$$

and

$$U_{O_2/Cd} = U_{O_2/OH^-} - U_{Cd(OH)_2/Cd} = 1.21V \quad [14c]$$

Equation [8] is a modified form of Ohm's law for the electrolyte which indicates that the curent in the electrolyte is driven by the electric potential gradient and the electrolyte concentration gradient. Equation [9] is Ohm's law for the solid phase. Equation [10] defines the transfer current that exists because of the electrode reactions which cause a gradient of the superficial current density in solution, $\partial i_2/\partial x$. Equation [11] is the material balance in the solid phase which describes the porosity changes with time due to the conversion of the active solid materials with different densities by the electrode reaction. Equations [12] and [13] are the mass balance of the electrolyte (KOH) and oxygen (O_2), which indicate that the electrolyte and the "effective" oxygen concentration at any position changes with time because of the electrode reaction and mass transfer. Mass transfer of OH^- is considered to be only diffusion and migration. Convection transport of OH^- is neglected. The exponents, ex1 and exm1, in these equations are tortuosity factors for the porous electrode. The concept of an effective oxygen concentration is used to provide a means of accounting for both gas and liquid phase transport of oxygen without including separately the gas phase and dissolved oxygen transport in the electrodes and the separator. The same concept applies to the apparent diffusion coefficient of oxygen, D_{O_2}. This is very important during overcharge process.

Interface between region 1 and 2.—

$$\epsilon_1^{ex1}\frac{\partial c}{\partial x}\bigg|_{region1} = (f_{sat}\epsilon_{sep})^{ex2}\frac{\partial c}{\partial x}\bigg|_{region2} \quad [15]$$

$$\frac{\partial \epsilon_1}{\partial t} = \frac{1}{\mathbf{F}}\left(\frac{M_{Ni(OH)_2}}{\rho_{Ni(OH)_2}} - \frac{M_{NiOOH}}{\rho_{NiOOH}}\right) j_{Ni} \quad [16]$$

$$i_2 = i_{cell} \quad [17]$$

$$\frac{\partial \phi_{1,Ni}}{\partial x}\bigg|_{region1} = 0 \quad [18]$$

$$\epsilon_1^{ex1}\frac{\partial \phi_2}{\partial x}\bigg|_{region1} = (f_{sat}\epsilon_{sep})^{ex2}\frac{\partial \phi_2}{\partial x}\bigg|_{region2} \quad [19]$$

$$\epsilon_1^{ex1}\frac{\partial c_{O_2}}{\partial x}\bigg|_{region1} = (f_{sat}\epsilon_{sep})^{ex2}\frac{\partial c_{O_2}}{\partial x}\bigg|_{region2} \quad [20]$$

Equations [15], [19] and [20] are in accordance with the continuity of the flux conditions of the electrolyte, superficial current density and oxygen at this interface. Equation [16] is the material balance in the solid phase. Equation [17] shows that all of the current through the cell is in the solution at this interface. Since the current in the solid phase is equal to zero, the potential gradient in the solid phase at this interface is also equal to zero, as given in Eq. [18].

*Region 2: separator.—*Ohm's law in the solution

$$\frac{i_2}{\kappa\epsilon_2^{ex2}} = -\frac{\partial \phi_2}{\partial x} + \frac{RT}{\mathbf{F}}(1-t_-^o)\frac{\partial \ln c}{\partial x} \quad [21]$$

Current in solution

$$i_2 = i_{cell} \quad [22]$$

Solid phase potential

$$\phi_1 = 0 \quad [23]$$

Porosity

$$\epsilon = f_{sat}\epsilon_{sep} \quad [24]$$

Electrolyte material balance

$$\epsilon\frac{\partial c}{\partial t} = D\epsilon^{ex2}\frac{\partial^2 c}{\partial x^2} \quad [25]$$

Oxygen material balance

$$\epsilon\frac{\partial c_{O_2}}{\partial t} = D_{O_2}\epsilon^{ex2}\frac{\partial^2 c_{O_2}}{\partial x^2} \quad [26]$$

Equation [21] again is a modified form of Ohm's law for the electrolyte, which is similar to Eq. [8] in the positive electrode region. Since the solid phase of the separator is not conductive, the current is carried totally by the liquid phase as shown in Eq. [22] and the potential of the matrix is arbitrarily set to zero, Eq. [23]. Equation [24] shows that the void space available to the electrolyte is equal to the porosity of the separator, ϵ_{sep}, times the level of liquid saturation in the separtor, f_{sat}. Finally, Eq. [25] and [26] are the material balance of the electrolyte and oxygen concentration.

Interface between region 2 and 3.—

$$(f_{sat}\epsilon_{sep})^{ex2}\frac{\partial c}{\partial x}\bigg|_{region2} = \epsilon_3^{ex3}\frac{\partial c}{\partial x}\bigg|_{region3} \quad [27]$$

$$\frac{\partial \epsilon_3}{\partial t} = \frac{1}{2\mathbf{F}}\left(\frac{M_{Cd(OH)_2}}{\rho_{Cd(OH)_2}} - \frac{M_{Cd}}{\rho_{Cd}}\right) j_{Cd} \quad [28]$$

$$i_2 = i_{cell} \quad [29]$$

$$\frac{\partial \phi_{1,Cd}}{\partial x}\bigg|_{region3} = 0 \quad [30]$$

$$(f_{sat}\epsilon_{sep})^{ex2}\frac{\partial \phi_2}{\partial x}\bigg|_{region2} = \epsilon_3^{ex3}\frac{\partial \phi_2}{\partial x}\bigg|_{region3} \quad [31]$$

$$(f_{sat}\epsilon_{sep})^{ex2}\frac{\partial c_{O_2}}{\partial x}\bigg|_{region2} = \epsilon_3^{ex3}\frac{\partial c_{O_2}}{\partial x}\bigg|_{region3} \quad [32]$$

where, on discharge and at rest

$$j_{Cd} = \alpha_{max3} i_{o3,ref}\left(\frac{c}{c_{ref}}\right)^{\gamma 3}\left(\frac{\epsilon_3 - \epsilon_{o3}}{\epsilon_{max3} - \epsilon_{o3}}\right)^{\zeta 3}\left\{\exp\left[\frac{\alpha_{a3}\mathbf{F}}{RT}\eta_c\right] - \exp\left[\frac{-\alpha_{c3}\mathbf{F}}{RT}\eta_c\right]\right\} \quad [33a]$$

and on charge

$$j_{Cd} = a_{max3} i_{o3,ref} \left(\frac{c}{c_{ref}}\right)^{\gamma 3} \left(\frac{\epsilon_3 - \epsilon_{o3}}{\epsilon_{max3} - \epsilon_{o3}}\right)^{\zeta 3} \left\{\exp\left[\frac{a_{a3}\mathbf{F}}{RT}\eta_c\right] - \exp\left[\frac{-\alpha_{c3}\mathbf{F}}{RT}\eta_c\right]\right\} \quad [33b]$$

and

$$\eta_c = \phi_{1,Cd} - \phi_2 \quad [33c]$$

Region 3: negative electrode.—The equations given below for the negative electrode are almost the same as those used in the positive electrode region.
Ohm's law in the solution

$$\frac{i_2}{\kappa \epsilon_3^{ex3}} = -\frac{\partial \phi_2}{\partial x} + \frac{RT}{\mathbf{F}}(1 - t_-^o)\frac{\partial \ln c}{\partial x} \quad [34]$$

Conservation of charge

$$i_2 - \sigma_{Cd}\epsilon_3^{exm3}\frac{\partial \phi_{1,Cd}}{\partial x} = i_{cell} \quad [35]$$

Transfer current

$$\frac{\partial i_2}{\partial x} = j_{Cd} + j_{O_2} \quad [35]$$

Porosity variation

$$\frac{\partial \epsilon_3}{\partial t} = \frac{1}{2\mathbf{F}}\left(\frac{M_{Cd(OH)_2}}{\rho_{Cd(OH)_2}} - \frac{M_{Cd}}{\rho_{Cd}}\right) j_{Cd} \quad [36]$$

Electrolyte material balance

$$\epsilon_3 \frac{\partial c}{\partial t} + c\frac{\partial \epsilon_3}{\partial t} = \frac{\partial}{\partial x}\left(D\epsilon_3^{ex3}\frac{\partial c}{\partial x}\right) - \left(\frac{1 - t_-^o}{\mathbf{F}}\right) j_{Cd} + \frac{t_-^o}{\mathbf{F}} j_{O_2} \quad [37]$$

Oxygen material balance

$$\epsilon_3 \frac{\partial c_{O_2}}{\partial t} + c_{O_2}\frac{\partial \epsilon_3}{\partial t} = \frac{\partial}{\partial x}\left(D_{O_2}\epsilon_3^{ex3}\frac{\partial c_{O_2}}{\partial x}\right) + \frac{1}{4\mathbf{F}} j_{O_2} \quad [38]$$

where the kinetic expression for oxygen reaction is

$$j_{O_2} = a_{max3} i'_{o3,ref} \left(\frac{\epsilon_3 - \epsilon_{o3}}{\epsilon_{max3} - \epsilon_{o3}}\right)^{\zeta 3} \left\{\exp\left[\frac{\alpha'_a \mathbf{F}}{RT}\eta'_c\right] - \left(\frac{c_{O_2}}{c_{O_2,ref}}\right)\exp\left[\frac{-\alpha'_c \mathbf{F}}{RT}\eta'_c\right]\right\} \quad [39a]$$

and

$$\eta'_c = \phi_{1,Cd} - \phi_2 - U_{O_2/Cd} \quad [39b]$$

Center of the negative electrode.—

$$\frac{\partial c}{\partial x} = 0 \quad [40]$$

$$\frac{\partial \epsilon_3}{\partial t} = \frac{1}{2\mathbf{F}}\left(\frac{M_{Cd(OH)_2}}{\rho_{Cd(OH)_2}} - \frac{M_{Cd}}{\rho_{Cd}}\right) j_{Cd} \quad [41]$$

$$i_2 = 0 \quad [42]$$

$$\frac{\partial i_2}{\partial x} = j_{Cd} \quad [43]$$

$$\frac{\partial \phi_2}{\partial x} = 0 \quad [44]$$

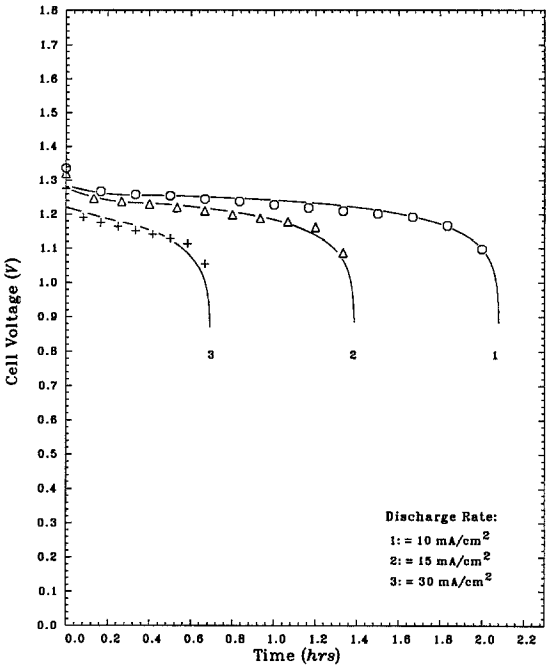

Fig. 2. Discharge characteristic of a nickel-cadmium cell

$$\frac{\partial c_{O_2}}{\partial x} = 0 \quad [45]$$

The equations used at this boundary are very similar to those at the center of the positive electrode except that the solid phase potential is already established so the transfer current condition is used instead of setting a value for ϕ_1.

The appropriate equations given above on discharge and rest or on charge were put into finite difference form and solved numerically using a pentadiagonal BAND(J) subroutine (14) and an implicit stepping technique for the time derivatives. The fixed parameters used in the calculations are given in Tables I-III. The parameter values given without references are assumed values. The simulated results are presented and discussed next.

Results and Discussion

Discharge characteristic.—The model simulated cell voltage *vs.* time curves for three discharge rates (solid

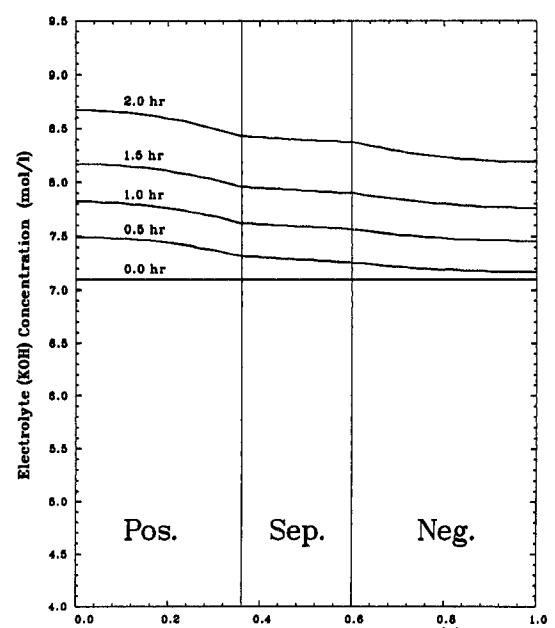

Fig. 3. Electrolyte concentration profiles at different discharge times

lines) and the corresponding experimental data [data points, refer to Ref. (15)] are shown in Fig. 2. It can be seen that the model has a very good fit to the experimental results. Both the model predictions and the experimental results indicate that the cell voltage drops quickly from the open-circuit potential (1.30V) to certain values at the beginning of discharge, then decays very slowly during the main course of discharge, and finally falls off upon complete discharge.

Figure 3 presents the profiles of the electrolyte concentration for a typical discharge process at a rate of 10 mA/cm^2, which is approximately a 2h rate. It indicates that the electrolyte concentration increases in all three regions. This increase is not due to the generation of OH^- in the electrode reaction, because OH^- does not appear in the overall cell reaction. Although OH^- is generated on the positive electrode according to reaction [A], it diffuses through the separator and is reduced on the negative electrode according to reaction [C]; therefore, the overall accumulation of OH^- due to the electrode reactions is simply zero. This increase in the electrolyte concentration is due to the overall water consumption. During discharge, water is consumed within the positive electrode region which directly causes the overall electrolyte concentration to increase. In addition, because of the generation of OH^- in the positive electrode according to reaction [A] and the consumption of OH^- in the negative electrode according to reaction [C], the increase of electrolyte concentration in the positive electrode is greater than that in the negative electrode.

Figure 4 presents the predicted porosity profiles of the solid materials as a function of time at a discharge rate of 10 mA/cm^2. As can be seen, the porosity of both electrodes decreases during discharge, because during discharge the electrode active materials are converted from their dense state, *e.g.*, NiOOH and Cd, to a loose state, *e.g.*, $Ni(OH)_2$ and $Cd(OH)_2$. The decrease in the solid material density will result in a decrease in the overall void volume. The porosity shows an almost uniform decrease across the electrode section; therefore, the electrode reaction rate is not a strong function of spatial position. This feature is quite different from that of those systems under diffusion control (8). This implies that the discharge process probably is under activation control but not under diffusion control.

Charge characteristic.—Figure 5 shows the simulated and experimental (15) values of the cell potential under three charge rates. Qualitative agreement again exists between the experimental and simulated values. Figure 6 shows that the electrolyte concentration continuously decreases during charge and overcharge due to production of water in the positive electrode. For a 1.5 recharge ratio (3h charge time/2h discharge time), the electrolyte concentration drops from about 8.5 mol/liter to about 6.4 mol/liter. Figure 7 indicates that porosity of both the positive and the negative electrode increases as expected. The porosity of the positive electrode returns to its original value gradually upon overcharge, but the porosity of the negative electrode continues to increase upon 1.0 recharge ratio and slightly passes through its original value (0.55). When the overcharge continues, the porosity quickly drops back to its original value (0.55), which is probably due to the time delay of oxygen diffusion.

The effect of oxygen is very important in a nickel-cadmium battery. The cell performance is greatly affected by the oxygen generation and reduction process. Here we assume that all oxygen exists only in the solution phase; and an apparent oxygen diffusion coefficient (D_{O_2}) and an effective oxygen concentration (c_{O_2}) are used to account for the two-phase transport of oxygen. As can be seen from Fig. 8, oxygen is generated on the positive electrode according to reaction [B], diffuses through the separator, and is reduced electrochemically on the negative electrode according to reaction [D]. Note that the oxygen builds up significantly in the positive electrode and reduces in the negative electrode region near the separator.

This process of oxygen reduction in the cell can be explained by constructing a simplified Evans plot for the

Table I. Properties of the electrolyte

Properties	Values	References
Cell temperature (T)	298.15 K	
Ref. basic concentration (c_{ref})	7.1 mol/liter	(2), p. 580
Ref. oxygen concentration ($c_{O_2,ref}$)	1.0 mol/liter	
Diffusion coefficient of KOH (D_{KOH})	2.13×10^{-5} cm^2/s	(2), p. 591
Diffusion coefficient of oxygen (D_{O_2})	1.00×10^{-3} cm^2/s	
Transference number (t°_-)	0.78	(2), p. 598
Electrolyte conductivity (κ)	0.67 S/cm	(2), p. 593

Table II. Electrode and separator properties

Properties	Positive (Region 1)	Separator (Region 2)	Negative (Region 3)	Reference
Half thickness (cm)	0.036	0.0125	0.040	(15)
Porosity (fully charged) (ϵ)	0.41	0.75	0.64	(2), p. 45
Maximum charge (Q_{max}, C/cm^3)	2082	—	3032	(12)
Surface area (α_{max}, cm^2/cm^3)	5600	—	5600	—
Tortuosity factors (ex/exm)	2.5/0.5	2.5	2.5/0.5	—
Saturation level (f_{sat})	—	0.9	—	—

Table III. Thermodynamic and kinetic parameters

Properties	Main reactions	Oxygen reaction	Reference
Open-circuit potential (V)	1.299	1.21	(2), p. 533
$i_{o1,ref}$ (A/cm^2)	6.1×10^{-5}	1.0×10^{-9}	(5), p. 15
$i_{o3,ref}$ (A/cm^2)	6.1×10^{-5}	1.0×10^{-9}	(5), p. 15
Number of electrons (n)	2	2	
α_{a1}	1.0	1.0	
α_{a3}	1.0	1.0	
α_{c1}	1.0	1.0	
α_{c3}	1.0	1.0	
$\gamma 1$	1.0	1.0	
$\gamma 3$	1.0	1.0	
$\zeta 1$	1.0	1.0	
$\zeta 3$	1.0	1.0	

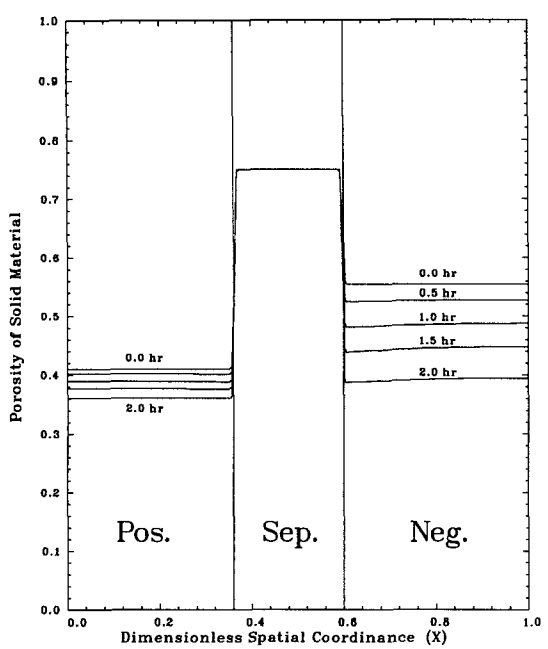

Fig. 4. Porosity profiles of solid material at different discharge times

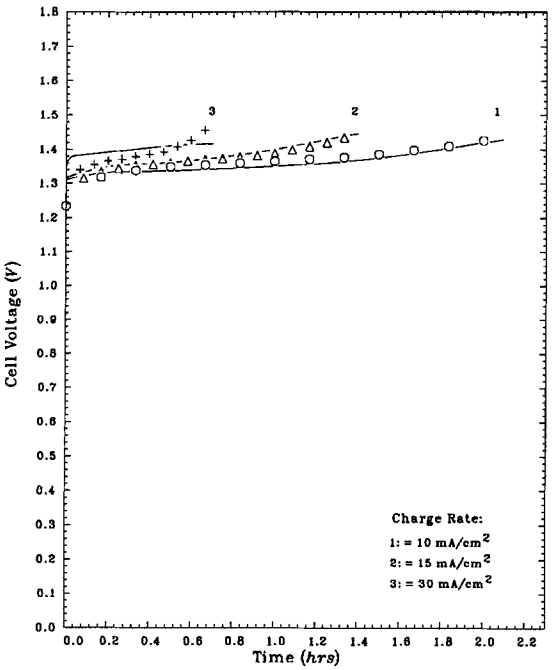

Fig. 5. Charge characteristics of a nickel-cadmium cell

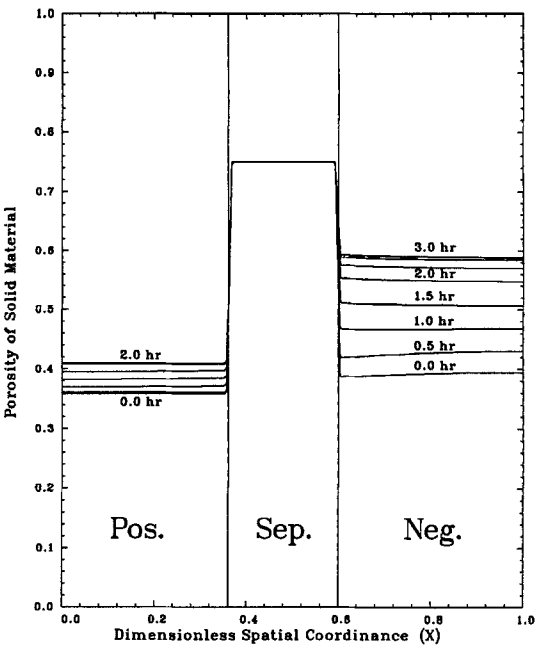

Fig. 7. Porosity profiles of solid material at different charge times

electrode reactions in the cell. Figure 9 is an Evans plot for the electrode reactions [A-D]. The parameters used in preparing this plot are listed in Table IV. It is important to note that Fig. 9 is only a qualitative representation of the actual electrochemical process in the model and in the cell, but it is consistent with the model predictions. During the charging period, oxygen generation on the positive electrode is along the positive branch ($\overline{AB}$) and the electrochemical reduction of oxygen on the negative electrode is along the negative branch ($\overline{ACD}$). This hypothesis is consistent with the results presented by Turner (16) in which he stated that oxygen recombination may be due to the electrochemical reduction of oxygen on the cadmium of the negative electrode and that the recombination rate depends upon the amount of metallic cadmium on the negative electrode. Further consideration of Fig. 9 reveals that it is highly unlikely that Cd is oxidized to $Cd(OH)_2$ during the charging process because cadmium is cathodically protected. This is true because on charge the potential of the negative electrode is lower than the equilibrium potential of the electrode reaction [C], which is obviously on the $Cd(OH)_2$ reduction branch of the Evans plot of the cadmium electrode part ($\overline{EF}$).

Voltage control charge characteristic.—In order to avoid pressure buildup due to oxygen generation during charge and overcharge, a voltage control charging technique is frequently used. In this charge mode, a constant charge current is applied at the beginning of charge when the cell voltage reaches a set value (1.35V) and is then changed to constant voltage charge, which allows the charge current to drop. This technique was developed based on the electrochemical phenomena shown in Fig. 9. According to Fig. 9, the entire process of oxygen generation, diffusion, and oxygen reduction is more likely to be controlled by diffusion of oxygen through the separator. If the charging rate is fast and the charging efficiency is low (*e.g.*, during overcharge), then the cell pressure will increase quickly due to oxygen generation. If a constant voltage is applied, the oxygen generation, diffusion, and reduction will reach

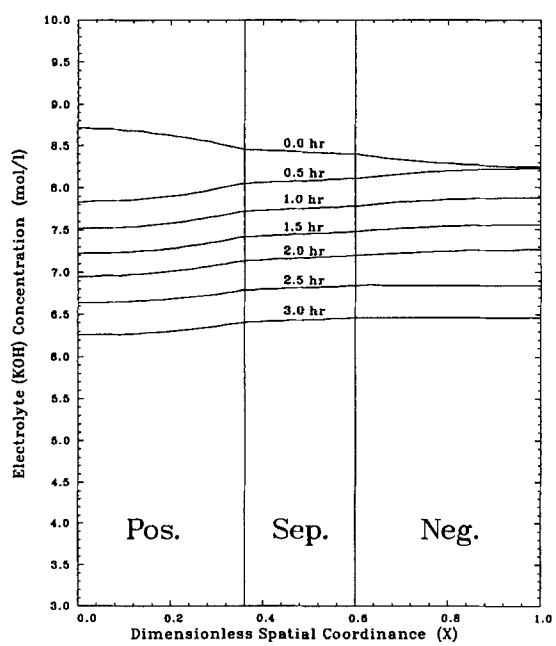

Fig. 6. Electrolyte concentration profiles at different charge times

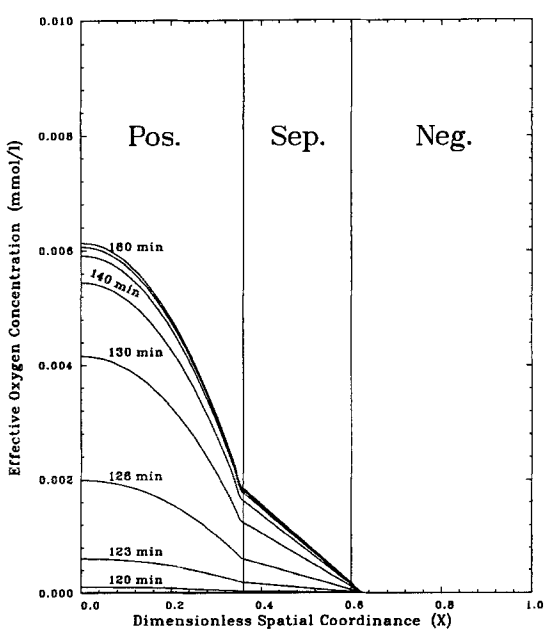

Fig. 8. Oxygen concentration profiles at different charge times

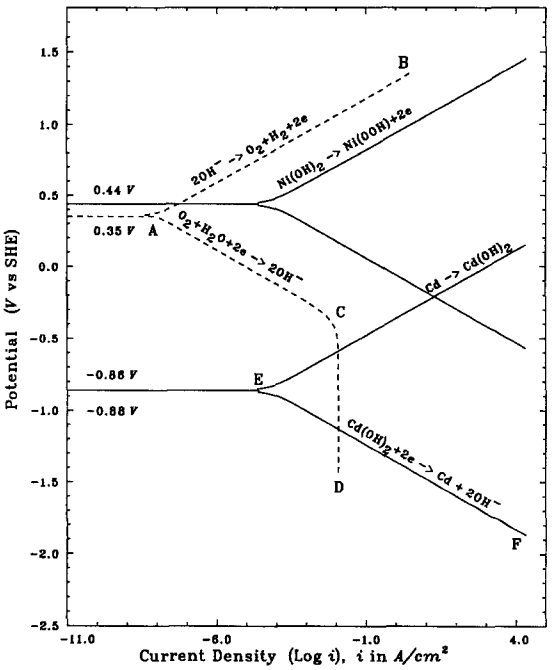

Fig. 9. Evans plot for the electrode reactions in a nickel-cadmium cell.

a steady state before the oxygen pressure builds up significantly. Figure 10 shows the charge current density as a function of time. If the oxygen reactions [B] and [D] are not included in the model, the charge current density will drop to zero during voltage control charge. This is a pure hypothetical case. If the oxygen reactions on both the positive and the negative electrodes are included in the model, the charge current density during voltage control charge approaches a nonzero asymptotic value, which indicates that oxygen generation, diffusion, and reduction reach a steady state in the cell. The oxygen concentration in the positive electrode for this charging technique is shown in Fig. 11. Comparison of Fig. 11 to Fig. 8 shows that the oxygen buildup during the voltage control charge is much less than that during the constant rate charge.

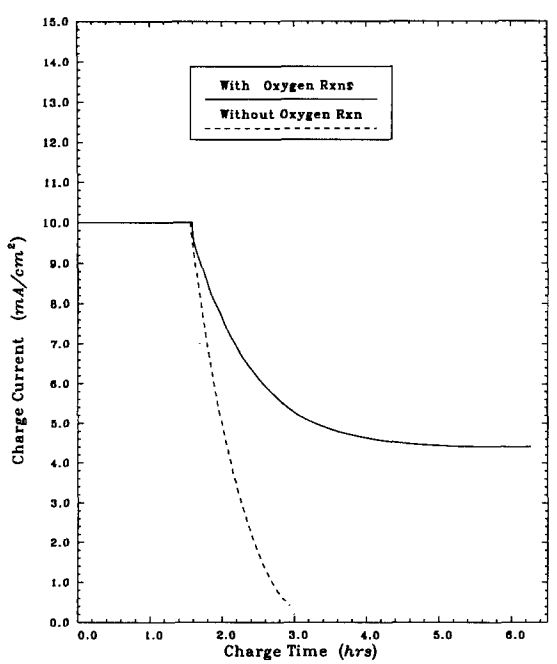

Fig. 10. Charge current density as a function of time for the voltage control charge mode (*i.e.*, first constant current charge at 10 mA/cm² until the voltage reaches 1.35, then constant voltage charge and current falls off).

Table IV. Parameters used in preparing the Evans plot

Electrode Active materials	Positive $NiOOH/Ni(OH)_2$	Negative $Cd(OH)_2/Cd$
i_o for main reaction (A/cm²)	6.1×10^{-5}	6.1×10^{-5}
i_o for oxygen reaction (A/cm²)	1.0×10^{-9}	1.0×10^{-9}
Equ. potential in 7.1*M* KOH (V)	0.44	−0.86
O_2 potential in in 7.1*M* KOH[a] (V)	0.35	0.35

[a] Refers to oxygen partial pressure as 1 atm.

Sensitivity analysis.—It is important to determine the sensitivity of the model predictions to changes in the electrode kinetic parameters and transport properties. If the model predictions are relatively insensitive to one or more parameters, then a fairly wide range of values for these parameters could be used without significantly affecting the predictions of the model. The sensitivity of the model predictions to changes in parameters is determined by monitoring the change in cell voltage. While holding all other parameters constant, the parameter of interest is perturbed slightly and the resulting change in cell voltage is noted. A sensitivity coefficient (SC) is defined as follows

$$SC_i = \frac{\sum_{j=1}^{n} |\Delta E(t_j)|}{n|\Delta par_i|/par_i^*} \quad [46]$$

where

$$\Delta E(t_j) = E(t_j) - E^*(t_j) \quad [47]$$

$$\Delta par_i = par_i - par_i^* \quad [48]$$

par_i and par_i^* are the perturbed values of parameter i and the reference value of parameter i, respectively. $E(t_j)$ is the value of the cell voltage at time t_j when using par_i; and, $E^*(t_j)$ is the value of the cell voltage at time t_j when using par_i^*. In Eq. [46], n is the number of times over which the voltage values are compared, and its value is chosen so that 80% of the discharge or charge time is included in the analysis.

The results of the sensitivity analysis are shown in Fig. 12 and 13. Figure 12 shows sensitivity of the cell voltage to the electrode kinetic parameters describing the dis-

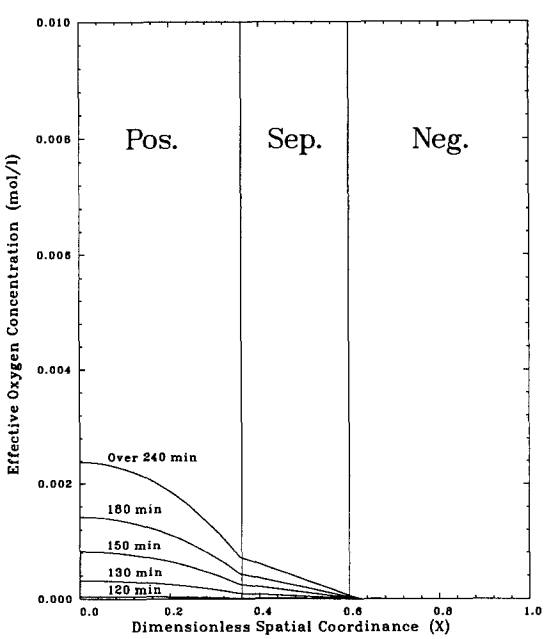

Fig. 11. Oxygen concentration profiles during the voltage control charge mode.

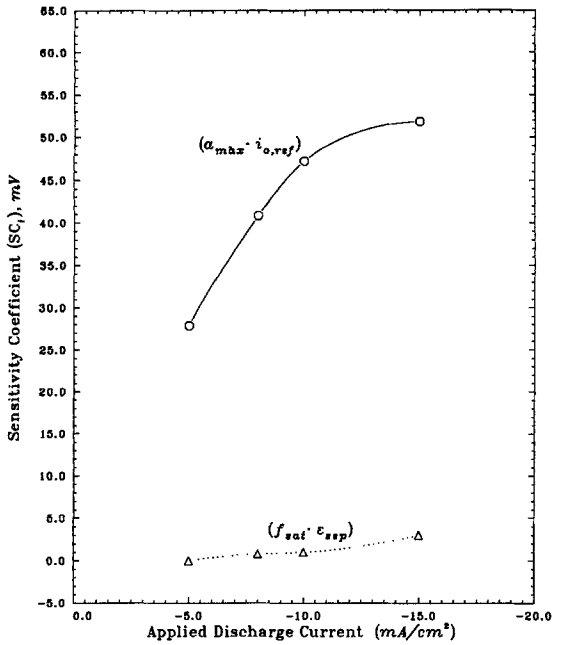

Fig. 12. Sensitivities of the predicted cell voltage to changes in the electrode kinetic parameter and separator property during the discharge processes.

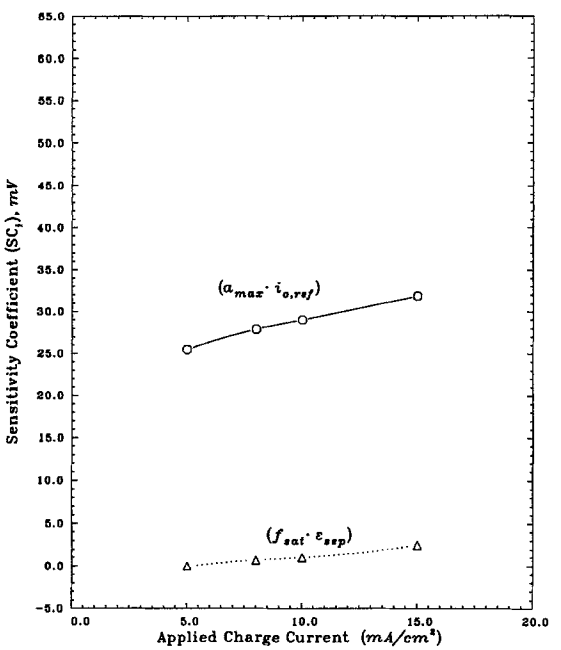

Fig. 13. Sensitivities of the predicted cell voltage to changes in the electrode kinetic parameter and separator property during the charge processes.

charge reaction over a range of discharge rates. Figure 13 is an analogous plot for the charging process. The kinetic parameter is represented by the product of exchange current density and the maximum specific surface area. The same values of exchange current density and specific surface area are used for both the positive and negative electrode (*i.e.*, $i_o \cdot a_{max} = i_{o1,ref} \cdot a_{max1} = i_{o3,ref} \cdot a_{max3}$). The transport parameter is characterized by the product of saturation level, f_{sat}, and the porosity of the separator, ϵ_{sep}. The sensitivity analyses indicate that the most influential factor by far is the electrode kinetics ($i_o \cdot a_{max}$), especially at high discharge or charge current density. The parameters characterizing the transport of the electrolyte through the separator have much less influence on the cell voltage during both the charge and discharge period. This indicates that the nickel-cadmium cell operates under activation control.

Future Model Refinement

The results presented here are some primary simulation results. Many other important features need to be incorporated into the model in order to have a better understanding of the electrochemical phenomena in a nickel-cadmium cell. Some future refinements to the model may include: (*i*) solid intercalation properties of the nickel electrode; (*ii*) semiconductor properties of the nickel electrode; (*iii*) proton diffusion in the nickel electrode (*iv*) two-phase transport of oxygen; (*v*) porosity distribution across the electrode section; and (*vi*) degradation effects.

Conclusions

A mathematical simulation for the discharge and charge performance of a sealed nickel-cadmium battery has shown that the model can be used to predict cell performance. Thus, it can serve as a useful tool for cell designers and engineers in studying the effect of various design parameters on the discharge and charge performance of the cell. The sensitivity analyses indicate that the product of exchange current density and specific surface area is the most influential factor to cell performance.

Acknowledgments

The authors acknowledge gratefully that this work was supported by the Jet Propulsion Laboratory (NASA) under Contract No. 958344. We would also like to thank Gerald Halpert, Paul Timmerman, Karla Clark, Sal DiStefano, and Peter Gluck for their helpful discussions and for providing many of the parameter values used in our model. Finally, we would like to thank Jet Propulsion Laboratory for use of their supercomputer and Cray Research, Inc., for time on the Cray YMP at Texas A&M University.

Manuscript submitted Dec. 18, 1989; revised manuscript received Aug. 7, 1990.

Texas A&M University assisted in meeting the publication costs of this article.

LIST OF SYMBOLS

$a_{max,j}$	maximum specific active surface area of region j, cm^2/cm^3 (j = 1, 3)
c	concentration of the binary electrolyte, KOH, mol/cm^3
c_{ref}	reference concentration of the binary electrolyte, KOH, mol/cm^3
c_{O_2}	effective oxygen concentration, mol/cm^3
$c_{O_2,ref}$	effective reference oxygen concentration, mol/cm^3
D_{KOH}	diffusion coefficient for KOH, cm^2/s
D_{O_2}	apparent diffusion coefficient of oxygen, cm^2/s
exj	tortuosity factors of porous media in region j for liquid properties (diffusion coefficients and conductivities) (j = 1, 2, 3)
exmj	tortuosity factors of region j for solid properties (conductivity) (j = 1, 3)
f_{sat}	level of electrolyte saturation in the separator
F	Faraday's constant, 96,487 C/mol
$i_{oj,ref}$	exchange current density of the reactions in region j at c_{ref}, A/cm^2 (j = 1, 3)
$i'_{oj,ref}$	exchange current density of oxygen reaction in region j at $c_{O_2,ref}$, A/cm^2
i_2	current density in solution based on the projected electrode area, A/cm^2
i_{cell}	applied current density based on the projected electrode area, A/cm^2
j	reaction current per unit volume of porous electrode, A/cm^3
j_{Ni}	nickel reaction current per unit volume of positive electrode, A/cm^3
j_{Cd}	cadmium reaction current per unit volume of negative electrode, A/cm^3
j_{O_2}	oxygen reaction current per unit volume of porous electrode, A/cm^3
l	total thickness of a cell unit, cm
l_1	half thickness of the positive electrode, cm
l_2	thickness of the separator matrix, cm
M_i	molecular weight of solid species i, g/mol i = NiOOH, $Ni(OH)_2$, Cd, $Cd(OH)_2$)
n_j	number of electrons involved in the electrode reaction j
par_i	perturbed values of parameter i
R	universal gas constant, 8.3143 J/mol-K
t	time, s
t^o_-	transference number of anion OH^- with respect to the solvent velocity

T absolute temperature, K
$U_{Ni/Cd}$ open-circuit potential of nickel-cadmium battery at c_{ref} = 7.1 mol/l, V
$U_{O_2/Cd}$ open-circuit potential of oxygen reaction with respect to cadmium electrode, V
U_i equilibrium potential for half reaction i at the reference state, V
x spatial distance from the center of the positive electrode, cm
X dimensionless distance from the center of the positive electrode, $X = x/l$

Greek letters

α_a, α_c anodic and cathodic transfer coefficients for the electrode reactions
α'_a, α'_c anodic and cathodic transfer coefficients for the oxygen reaction
γ exponents for the concentration dependence of reaction rate
ϵ_j porosities of solid materials of region j, (j = 1, 2, 3)
ϵ_{oj} porosities of solid materials of region j at zero charge, (j = 1, 3)
ϵ_{maxj} porosities of solid material of region j at full charge, (j = 1, 3)
ϵ_{sep} porosity of the separator matrix
ζ exponents for the active material dependence of reaction rate
κ electrolyte conductivity, S/cm
ρ_i densities of the solid material i, g/cm^3 (i = NiOOH, $Ni(OH)_2$, Cd, and $Cd(OH)_2$)
σ_i conductivities of the solid material, S/cm (i = NiOOH, Cd)
ϕ_1 potential in the solid phase, V
ϕ_2 potential in the liquid phase, V

Subscripts

1 positive electrode region
2 separator region
3 negative electrode region
O_2 oxygen or oxygen reaction
Ni positive electrode reaction [A]
Cd negative electrode reaction [C]

REFERENCES

1. P. McDermott, G. Halpert, S. Ekpanyaskun, and P. Nche, "Secondary Aerospace Batteries and Battery Materials," NASA SP-7044, July 1976.
2. S. U. Falk and A. J. Salkind, "Alkaline Storage Batteries," p. 45, John Wiley and Sons, Inc., New York (1969).
3. W. R. Scott and D. W. Rusta, "Sealed-Cell Nickel-Cadmium Battery Application Manual," NASA Reference Publication No. 1052, December 1979.
4. F. V. Sturm, "Comprehensive Treatise of Electrochemistry," Vol. 3, J. O'M. Bockris, B. E. Conway, E. Yeager, and R. E. White, Editors, Chap. 13, Plenum Press, New York (1981).
5. K. W. Choi and N. P. Yao, in "Battery Design and Optimization," PV 79-1, S. Gross, Editor, p. 62, The Electrochemical Society Softbound Proceedings Series, Princeton, NJ (1979).
6. H. Gu, T. V. Nguyen, and R. E. White, *This Journal*, **134**, 2953 (1987).
7. J. Bouet, F. Richard, and Ph. Blanchard, in "Nickel Hydroxide Electrodes," PV 90-4, D. A. Corrigan and A. H. Zimmerman, Editors, p. 260, The Electrochemical Society Softbound Proceedings Series, Pennington, NJ (1990).
8. T. V. Nguyen, R. E. White, and H. Gu, *This Journal*, **137**, 2998 (1990).
9. G. Linder, "Sealed Nickel-Cadmium Batteries," Varta Batterie AG, VDI-Verlag (1982).
10. A. H. Zimmerman and P. K. Effa, *This Journal*, **131**, 709 (1984).
11. J. Desitvestro, D. A. Corrigan, and M. J. Weaver, *ibid.*, **135**, 887 (1988).
12. S. U. Falk, *ibid.*, **107**, 633 (1960).
13. D. F. Pickett, H. S. Lim, S. J. Krause, and S. A. Verzwyvelt, *J. Power Sources*, **22**, 243 (1988).
14. J. Van Zee, G. Kleine, R. E. White, and J. S. Newman, "Electrochemical Cell Design," R. E. White, Editor, Plenum Press, New York (1984).
15. P. Timmerman, JPL, Private communication.
16. D. R. Turner, *Electrochem. Technol.*, **2** (11-12), 313 (1964).

Effect of Benzotriazole on Surface Processes during Copper Electrodissolution in Sulfuric Acid

Claude Clerc[1] and Richard Alkire*

Department of Chemical Engineering and Materials Research Laboratory, University of Illinois, Urbana, Illinois 61801

ABSTRACT

Impedance spectra were obtained during anodic dissolution of copper in 0.5*M* H_2SO_4 and 40 m*M* benzotriazole (BTA) at 25°C. The spectra were evaluated according to the hypothesis that the electrode is covered with a barrier film having a stoichiometric composition through which the current is transported by ionic conduction. This barrier film is itself covered with an outer porous film of corrosion products. The experimental impedance spectra were fit to the model with a nonlinear least squares program. A detailed analysis of the physical parameters obtained with this procedure suggested that the metallic ions transfer through the barrier film, which is likely to be hydrated copper sulfate or contains a nonnegligible amount of BTA, under high-field conduction. Experiments carried out at the mass-transfer limiting current in the absence of BTA suggested that the electrode was also covered with a similar dual salt film, the inner layer of which, however, has a different chemical composition than in the presence of BTA.

The presence of a surface film is a significant feature in virtually all cases of high-rate electrodissolution of a metal. Important practical applications of such phenomena include pitting corrosion (1-3), passivity (4), corrosion inhibition (5), electropolishing (6), and battery operations (7). Improved fundamental understanding of such surface films is therefore of widespread interest. Since such surface films respond to the unique conditions of the electrochemical environment in which they exist, *in situ* methods of characterization are strongly preferred. In the present work impedance spectroscopy was used.

In a recent study of copper dissolution in sulfuric acid, Alkire and Cangellari (8) showed that a small amount of benzotriazole (BTA), an organic inhibitor, promotes the precipitation of a surface film having a dual structure. According to this view, presented in Fig. 1a, there is a thin barrier film next to the metal which is covered by an outer porous film. From a series of potential step measurements at a rotating disk electrode, they concluded that the metallic ions transferred through the barrier film under high-field conduction, and that deviation from the mass-transfer rate predicted by the Levich equation was due to the porous film. A theoretical model was developed to describe the transport of the electrochemical species, assuming molecular diffusion and migration across the porous

* Electrochemical Society Active Member.
[1] Present address: Medinvent SA, Lausanne, Switzerland.